IEEE/CSC & ESAS European Superconductivity News Forum (ESNF), No. 15, January 2011
The published version of this manuscript appeared in *IEEE Transactions on Applied Superconductivity* **21**, Issue 3, 3132 - 3137 (2011)

Test Results of a NbTi Wire for the ITER Poloidal Field Magnets: A Validation of the 2-pinning Components Model

L. Muzzi, G. De Marzi, C. Fiamozzi Zignani, U. Besi Vetrella, V. Corato, A. Rufoloni, and A. della Corte

***Abstract*—A two-components model has been recently developed, for describing the normalized bulk pinning force curves and the critical current density of NbTi strands over a wider B-T range with respect to conventional single-component models. The model was previously successfully applied to data collected on several NbTi commercial strands, with different size, Cu:nonCu ratio, filament diameter and layout, thus confirming the presence of two different pinning mechanisms in conventionally processed NbTi wires. For a further validation, we have extensively tested a strand recently produced by the Chinese Company Western Superconducting Technologies for the ITER Poloidal Field (PF) magnets PF2 to PF5, and applied the model to these data. In order to take into account the observed non-scaling with temperature of the reduced pinning force curves, the model has been updated, including the observed difference in the temperature dependences of the two components contributing to the overall bulk pinning force. The importance of testing wires over very wide temperature ranges is evidenced, and the good agreement between experimental and fit results validate the proposed formulation, which can be regarded as a reliable tool for the description of NbTi performances, to be used in the design of superconducting magnets. From the phenomenological point of view, it is shown that at low temperatures, the two pinning mechanisms contribute to the bulk pinning force, resulting in a pinning force peaking at a reduced field $B/B_{irr} \cong 0.5$. As the temperature increases, the pinning force peak moves to lower fields, indicating that the low field component pinning mechanism becomes dominant.**

***Index Terms*—ITER, critical current density, magnetic characterization, transport measurements, superconducting NbTi strands.**

I. Introduction

The design of superconducting magnets based on NbTi strands, relies on the knowledge of their performances in the magnetic and temperature range of interest. In particular, the design of fusion magnets, usually based on Cable-in-Conduit conductors, and the requirement of the minimum temperature margin, translates into a requirement for the basic NbTi wires of minimum superconducting performances at relatively high magnetic field and temperature, typically in the range $B \sim 5$ T to 6 T, $T \sim 6.0$ K to 6.5 K [1]-[6]. As already shown and discussed [7]-[9], the prediction of strand performances in this range, can hardly be inferred from simple tests at, for example, liquid helium temperature. In addition, once a candidate wire has been tested in the proper *B, T* range, a fitting / scaling formula is required, in order to define and validate a conductor design.

The Luca Bottura scaling formula [10] has been widely and successfully applied in this sense. However, it doesn't allow an accurate description of NbTi complete data sets, as collected over wide B, T ranges. This is not necessarily a strict limitation, as long as the range of validity for a specific parameter set is kept limited to specified design operating ranges. However, the difficulty in extending the range of validity of such formulations, indicates that some aspects in the understanding of the behaviour of conventionally processed NbTi wires are probably missing.

Motivated by these considerations, we recently formulated the 2-pinning components model [11], based on the assumption that two pinning mechanisms are dominantly acting in these systems, that allowed us to accurately describe the performances of technological strands for fusion over a complete magnetic field range, and in the temperature range 4.2 K to 6.5 K. However, the model, as formulated up to now, could not take into account a possible temperature non-scaling of the reduced pinning force curves, whereas recent extensive tests carried out on a strand produced for the ITER PF magnets up to 8.5 K, revealed the expected temperature non-scaling. The fitting model has thus been upgraded, in order to take into account the observed phenomenology.

In the present paper, we first extensively report on the strand test results, and then illustrate the upgraded formulation of the 2-pinning components model, showing that a very good agreement with experimental data can now be achieved over the complete temperature and magnetic field range.

II. Sample

The NbTi strand sample analyzed in this work has been produced by the Chinese Company Western Superconducting Technologies (WST), and it is intended for the ITER low field

Manuscript received August 03, 2010.

The authors are with EURATOM-ENEA Association, ENEA C.R. Frascati, 00044 Frascati (Rome), Italy (corresponding author: L. Muzzi, ph: +39-0694005391; fax: +39-0694006119; e-mail: luigi.muzzi@enea.it).

magnets PF2 to PF5. Its nominal features are summarized in Table I, according to the ITER requirements for the NbTi strands *Type 2* [1]. The present strand has also been used in the cable of the first ITER PF2 qualification conductor [12], recently tested at the SULTAN facility in CRPP (CH) [13].

TABLE I
MAIN FEATURES OF THE TESTED NBTI STRAND SAMPLE. MEASUREMENTS PERFORMED: (I) BY SEM; (II) BY MAGNETIZATION; (III) BY TRANSPORT.

	Nominal	Measured
Supplier	WST (China)	
Strand ref. number	1012-08004-2580D2	
Strand Diameter	0.73 mm	0.729 ± 0.002 mm (i)
Filament Diameter	≤ 8 μm	7.7 ± 0.2 μm (ii + iii)
Cu:nonCu ratio	2.3	n/a
External Ni Coating thickness	2 μm	1.1 ± 0.1 μm (i)
Twist Pitch length	15 mm	n/a
Critical current at 5 T-4.2 K	> 339 A	348.7 A (iii)
Hysteresis losses per strand volume (4.2 K ; ±1.5 T cycle)	< 45 mJ/cm^3	39 mJ/cm^3 (ii)

III. Experimental Characterizations

An extended characterization of the strand has been performed. Both structural properties (strand diameter, thickness of external coating), as well as superconducting performances, in terms of electrical properties (transport critical current density at variable temperature) and magnetic properties (hysteresis losses in ±1.5 T magnetic field cycles), have been investigated.

A. Scanning Electron Microscope analysis

Short samples have been impregnated with resin and the surface accurately worked with lapping paste, in order to obtain sufficiently clean surfaces, to be analyzed by Scanning Electron Microscope (SEM). From SEM micrographs the strand diameter has been directly measured, as well as the thickness of the Ni outer layer. All results of SEM characterizations are reported in Table I, and are in good agreement with the nominal values. An example of the acquired SEM cross-sections is reported in Fig. 1.

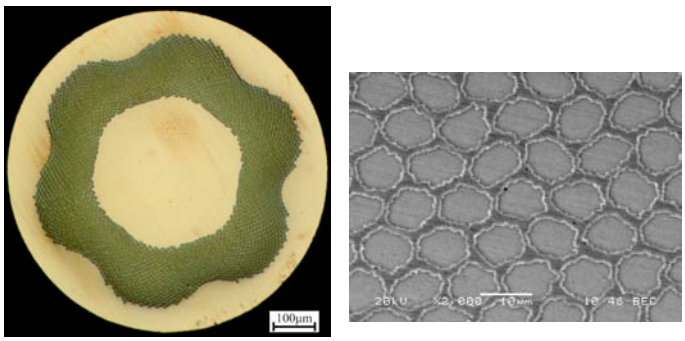

Fig. 1. Images of the WST 2580D2 NbTi wire: overall cross-section by optical microscope (left) and a zoom of the filamentary zone by SEM (right). Courtesy of Li Jianfeng (WST).

B. Electrical characterizations

The transport critical current has been measured on the sample, using a facility for measurements in liquid helium as function of magnetic field, as well as the Variable Temperature Insert (VTI) [14] for I_c measurements as function of temperature. On the first one, about 1.5 m of sample length is wound on a standard Ti6Al4V ITER barrel and critical current and transition *n-index* are determined, following standard procedures, in the magnetic field range 3 T to 10 T. As far as the VTI is concerned, the sample is wound on a steel sample holder, and its performances are characterized in the temperature range 4.2 K to 8.0 K. The result of the reference 5 T point is reported in Table I, whereas a plot of the collected I_c vs. field and *n-index* vs. I_c data are reported in Figs. 2 and 3 respectively.

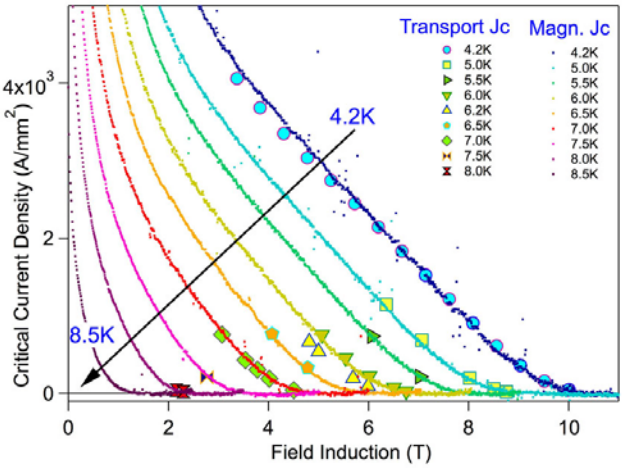

Fig. 2. Superconductor transport current density (symbols), compared to results extracted from magnetization data (see next section) as function of the magnetic field, in the temperature range 4.2 K to 8.5 K.

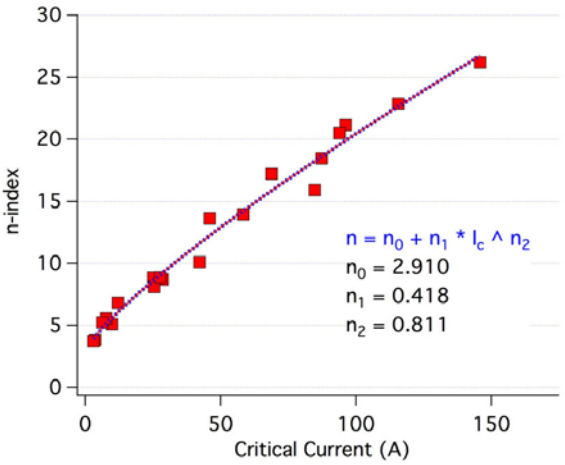

Fig. 3. Transition *n-index* determined in the range 0.1 to 1 μV/cm, as function of the critical current values. The characteristic curve is fitted by a power law, with the coefficients reported in the figure inset.

Table II reports the result of I_c measurements carried out at 6.2 K, as compared with the requirements for the conductor performances [1]. As one can see, the strand alone meets the requirements defined by the temperature margin in the PF2 to

PF4 conductors, within the experimental error, whereas the magnet PF5 might present some uncertainty in terms of design temperature margin with the present strand. However, the strand test doesn't provide a definitive answer in this sense, since only tests carried out on the full-size conductor at the nominal operating conditions, could verify these requirements. As a matter of fact, tests recently carried out on the ITER PF2 qualification conductor, manufactured using the here presented wire, have shown that full-size conductor T_{cs} performances might overcome the properties of the constituting strand, as considered at the peak magnetic field inside the conductor during test conditions [15]. The same result was also observed during the tests of the ITER Poloidal Field model coil (PFCI, Poloidal Field Conductor Insert) [16], and on the smaller NbTi qualification conductor for the JT-60SA TF magnet [2].

TABLE II
COMPARISON BETWEEN STRAND TESTS AND ITER REQUIREMENTS ON THE PERFORMANCES OF THE PF2-5 CONDUCTORS AT 6.2K

Coil	Design requirements				Measured strand data
	Conductor I_{op}	Strand I_{op}	Ref. Field B_{ref}	Min. T_{cs}	I_c at B_{ref} and T = 6.2 K
PF2-4	55 kA	76.4 A	4.8 T	6.2 K	84.7 A
PF2-4	50 kA	69.4 A	5.0 T	6.2 K	68.8 A
PF5	52 kA	45.1 A	5.7 T	6.2 K	25.4 A
PF5	33 kA	28.6 A	6.0 T	6.2 K	12.0 A

C. *Magnetization measurements*

Hysteresis losses have been determined from magnetization cycles measured by Vibrating Sample Magnetometer (VSM). The measurements have been performed at 4.2 K in ±1.5 T transversal field cycles, with a field variation rate of 0.4 T/min (~7 mT/s) and using a vibrating amplitude and frequency of, respectively, 0.2 mm and 45 Hz. In our system, samples for losses measurements are as small as about 3.5 mm long, in order to have the system operating in the magnetic dipole approximation, thus avoiding any appreciable effect due to demagnetization. Fig. 4 shows the magnetization cycles measured at 4.2 K, as well as at 6.5 K, referred to the total strand volume. More complete magnetization cycles, up to 12 T orthogonal field and at different temperatures, have been carried out as well, thus allowing us to extract the critical current density of the sample by means of the Bean model [17]. The very good agreement found between transport and magnetization measurements, as shown in Fig. 2, supports the use of this technique. In this sense, magnetization represents a very powerful tool, in order to extract the superconducting performances of technological wires, over a much wider field and temperature range with respect to the one that can be explored by transport characterizations. In addition, the comparison between transport and current data allows to determine the effective filament diameter, d_{eff}, through the following formula [18]:

$$J_c(A/cm^2) = \frac{30\pi}{4} \cdot \frac{\Delta m\ (emu/cm^3)}{d_{eff}(cm)} \cdot (1+\lambda) \qquad (1)$$

where J_c represents the superconductor critical current density, Δm the width of the magnetization cycle, and λ is the strand Cu:nonCu ratio. The main strand properties extracted from magnetization measurements, i.e. hysteresis losses and effective filament diameter, are reported in Table I.

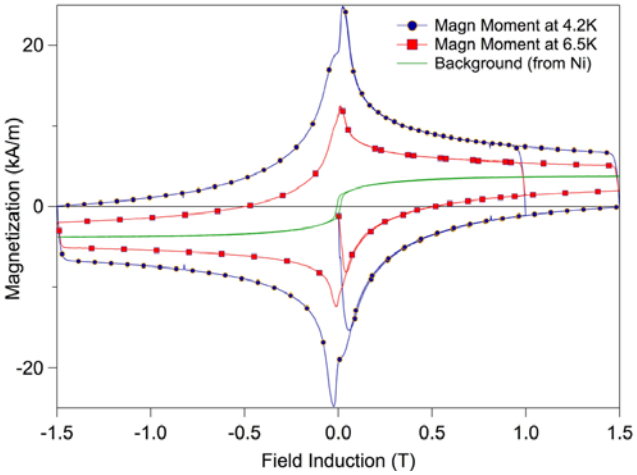

Fig. 4. Magnetization cycles measured at 4.2 K and 6.5 K, with a magnetic field ramp of about 7 mT/s, referred to the total strand volume. The different curve symbols are explained in the figure inset.

IV. DATA ANALYSIS BY MEANS OF THE 2-PINNING COMPONENTS MODEL

Using the transport and magnetization data reported in Fig. 2, it is possible to compute the experimental pinning forces at different temperatures, as the product of the critical current density and the magnetic field. In particular, Fig. 5 reports the normalized pinning force curves, measured between 4.2 K and 8.5 K, as function of the reduced field $b=B/B_{irr}$, B_{irr} being the irreversibility field. A relevant temperature non-scaling is observed, opposite to what was deduced in the past on different wires [7], [11], characterized in a more restricted temperature range (only up to 6.5 K). The corresponding values for B_{irr}, as determined by magnetization cycle closure points, and the pinning force maxima (F_{p_max}), are reported in Table III.

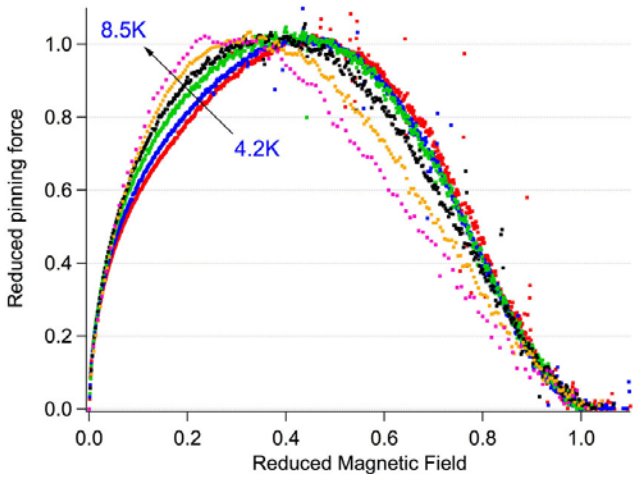

Fig. 5. Reduced pinning force vs. reduced field curves, measured in the temperature range 4.2 K to 8.5 K (0.46 T_c to 0.92 T_c).

TABLE III
PINNING FORCE MAXIMA AND IRREVERSIBILITY FIELDS, DETERMINED ON THE WST 2580D2 WIRE, AS FUNCTION OF TEMPERATURE

Temperature (K)	F_{p_max} (GN/m^3)	B_{irr} (T)
4.2	15.2	10.2
5.0	11.0	8.8
5.5	8.8	7.8
6.0	6.5	6.6
6.5	4.9	5.6
7.0	3.5	4.6
7.5	2.1	3.3
8.0	1.1	2.2

As regards the description in terms of the 2 pinning-components model, the observed temperature non-scaling shown in Fig. 5 can be considered as an indication that the 2 concurring pinning mechanisms have a different temperature dependence. Using the formulation proposed, for example, by Fietz and Webb [19], the pinning force for a specific mechanism can be written in the following factorized form:

$$F_p \propto B_{C2}^{\gamma}(T)\ b^{\alpha}\ (1-b)^{\beta} \qquad (2)$$

where the temperature dependence is enclosed within the dependence on the upper critical field, B_{c2}, through the parameter γ, whereas the dependence on the reduced field is described by the parameters α and β. Following the assumption of the 2-pinning components model, that two pinning force expressions can be directly summed up, the overall bulk pinning force F_p can be written as follows:

$$F_p = F_p^{(1)} + F_p^{(2)} = \\ = C_1 \cdot (1-t^n)^{\gamma_1} \cdot b^{\alpha_1} \cdot (1-b)^{\beta_1} + C_2 \cdot (1-t^n)^{\gamma_2} \cdot b^{\alpha_2} \cdot (1-b)^{\beta_2} \qquad (3)$$

with reduced field and temperature defined as follows [20]:

$$b = \frac{B}{B_{irr}(T)} = \frac{B}{B_{irr\_0}(1-t^n)}; \quad t = \frac{T}{T_{c0}} \qquad (4)$$

B_{irr_0} being the value of the upper critical field at zero temperature and T_{c0} the value of the critical temperature at zero field. By means of the expression (3), the J_c curves as function of field can be well fitted in the whole temperature range, up to 8.5 K. In particular, the complete $J_c(B,T)$ dataset is globally fitted by RMS minimization, and constraining B_{irr_0} and T_{c0} to vary between physically acceptable values. The result is shown in Fig. 6, where magnetization and transport J_c data are compared to fit results.

In order to clarify the way in which the different mechanisms contribute to the overall pinning force, Fig. 7 reports the reduced pinning force curves as function of the reduced magnetic field, at 4.2 K and at 7.0 K. Experimental data are compared to fit results, and the single pinning forces of the two components are evidenced. The pinning force peak shifts to lower reduced field values with increasing temperature, which is reflected in the fact that the weight of the low field (LF) component, characterized by a peak at a reduced field $b \cong 0.25$, increases with respect to the weight of the high field (HF) one, characterized by a peak at $b \cong 0.6$.

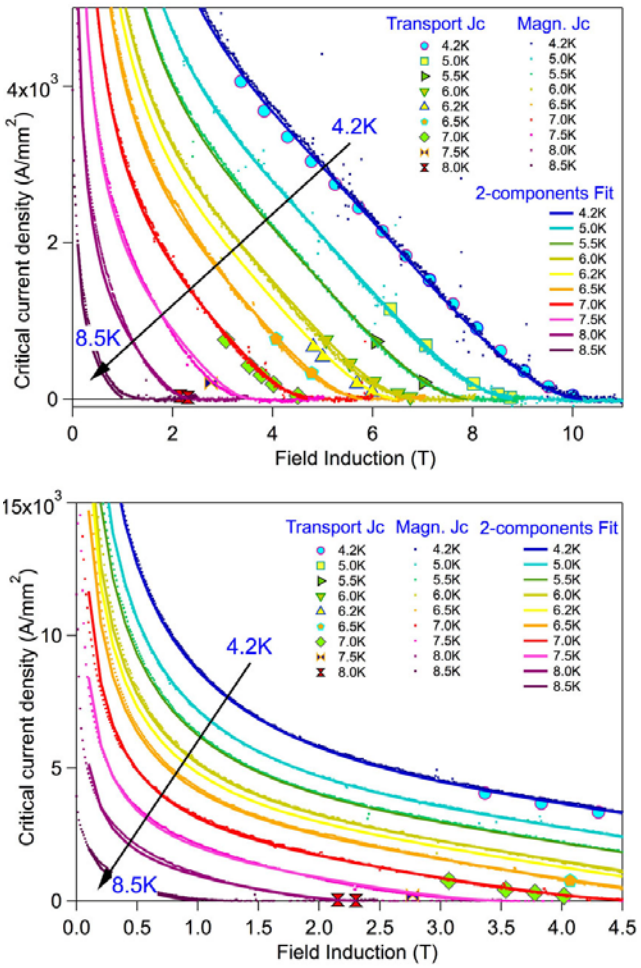

Fig. 6. Superconductor transport (large symbols) and magnetization (small symbols) current density as function of the magnetic field, in the temperature range 4.2 K to 8.5 K. Different J_c / B ranges are considered in the upper and in the lower plot, in order to better appreciate the fit results.

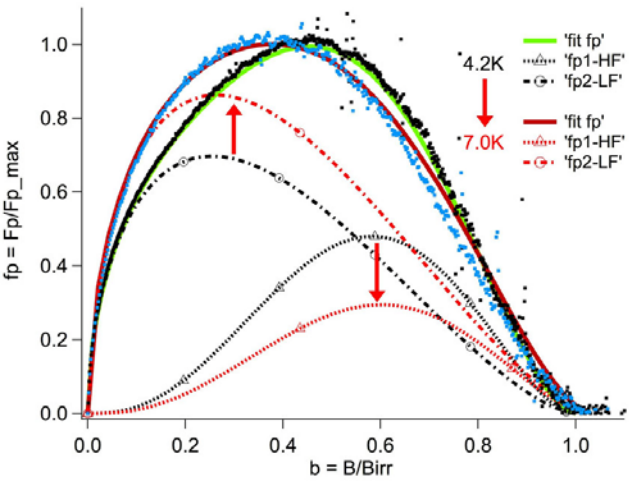

Fig. 7. Reduced pinning force curves at 4.2 K and 7.0 K. Experimental results (small symbols) are compared with fit results (continuous line); the shape of the 2 single pinning components, the sum of which provides the overall pinning curve, is evidenced (dash-dotted line for the LF component, dotted line for the HF one).

TABLE IV
PARAMETER SET FOR THE 2-PINNING COMPONENTS MODEL DESCRIPTION OF THE ITER WST 2580D2 AND JT-60SA LUVATA C2 WIRES

Fit parameter	ITER WST 2580D2	JT-60SA Luvata C2
T_{C0} (K)	8.908	8.955
B_{irr_0} (T)	14.156	14.211
α_1	2.714	3.068
β_1	1.951	2.111
α_2	0.542	0.621
β_2	1.584	1.935
γ_1	2.564	2.088
γ_2	1.646	1.817
C_1 (GN/m^3)	396	423
C_2 (GN/m^3)	60	67
Exp. b_m (4.2K / 8.5K)	0.45 / 0.29	0.49 / 0.32
b_{m1}	0.58	0.59
b_{m2}	0.25	0.24

The same fit procedure has been applied also to the data of the Luvata *C2* NbTi strand, candidate for the JT-60SA TF magnet [7], that has been recently re-tested, in order to extend, also for this strand, the range of available data up to a temperature of 8.5 K, thus allowing a more reliable test-bed for the model validation. Table IV reports the list of the best fitting parameters for the two wires. In addition, the reduced field at which the pinning force curve experimentally peaks, b_m, is indicated in the Table. This parameter depends on temperature, as already shown in Fig. 5, and it is slightly different for the two wires. On the other hand, the reduced fields at which the single pinning components peak, b_{m1} and b_{m2}, are practically identical for the two wires. In addition, they do not depend on temperature, in the sense that the position of the relative maxima do not vary with temperature. On the other hand, what provides the temperature dependence (and non-scaling) of the characteristic curves is the relative weight of the two pinning components, as already illustrated in Fig. 7.

As regards the origin of the two pinning mechanisms, it is not clear yet what they could be ascribed to. As discussed in [11], we believe that the two possible types of strong pinning defects might be identified with clusters of *α-Ti* ribbons [21], dominating at low reduced fields, and to Nb / Ti concentration gradients present around them [22], responsible for the behavior at high reduced fields.

Some hints on the possible nature of the pinning mechanisms can be obtained observing that dual pinning mechanisms have been also observed on YBCO High Temperature Superconducting films [23]-[24], characterized by the artificial introduction of nano-scale inclusions.

With the aim of clarifying the system behavior, we are currently analyzing data taken on a commercial, optimized NbTi strand, that has been subjected to dedicated annealing treatments. Transmission Electron Microscope (TEM) analyses are being performed on this sample set, in order to clarify the role of the microstructure and of possibly different concentration gradients on its pinning properties.

V. CONCLUSIONS

The NbTi wires intended to be used in the design of a superconducting fusion magnet should be characterized in temperature and magnetic field ranges as wide as possible; not only this allows to define in a reliable way suitable fitting formulas, but also helps in the interpretation of the pinning mechanisms that determine the performances of technological strands. In this sense, magnetization measurements represent a very powerful tool, since the characterization of wire properties can be extended in wider range, with respect to transport characterization, practically allowing to reconstruct complete pinning force curves.

We have widely characterized a multi-filamentary strand optimized for the ITER PF2 to PF5 magnets. The results show that the reduced pinning force curves do not scale with temperature.

Based on this observation, we upgraded the 2-pinning components model, with respect to its original formulation, and it can now accurately describe data in the complete magnetic field and temperature range. This result suggests that this model can be regarded as a useful tool in the design of magnets based on conventionally processed optimized wires, that can in principle be applied as a predictive tool, based for example on two independent measurements at sufficiently distant temperatures (e.g. 4.2 K and 8.0 K).

In the analyzed optimized wires for fusion applications the experimental pinning force maxima lie at a reduced field $b \cong 0.45$ to 0.5, gradually shifting to lower values with increasing temperature.

According to the proposed model, two types of pinning centres are mainly operating, or two different mechanisms, with their relative contribution to the total pinning force

changing with temperature. In particular, the relative maxima, at $b \cong 0.25$ and $b \cong 0.6$ for both analyzed wires, do not shift with temperature, whereas the weight of the low field pinning component becomes gradually dominant with increasing temperature, with respect to the high field one.

It should be also observed that the characterized wire meets the requirements for the NbTi *type 2* strands for the ITER PF2 to PF4 conductors, whereas strand performances are below the requirements for the PF5 conductor at the peak magnetic field: in this case, a full-size conductor test should be foreseen, in order to assess whether the design temperature margin can be maintained at the presently foreseen level of 1.5 K.

ACKNOWLEDGMENT

The authors acknowledge Alex Vostner (ITER IO) for strand supply, Li Jianfeng (WST) for useful suggestions and Liu Bo, Andrea Augieri, and Giuseppe Celentano for fruitful discussions.

REFERENCES

[1] ITER Design Description Document DDD11–7: Conductors, ITER_D_2NBKXY v1.2, Sept. 2009.

[2] L. Muzzi et al., “The JT-60SA Toroidal Field conductor Reference Sample: manufacturing and test results”, *IEEE Trans. On Appl. Supercond.*, *IEEE Trans. on Appl. Supercond.*, vol 20, no. 3, pp. 442-446, 2010.

[3] K. Kizu et al., “Conductor Design of CS and EF Coils for JT-60SA”, *IEEE Trans. On Appl. Supercond.*, *IEEE Trans. on Appl. Supercond.*, vol 18, no. 2, pp. 212-215, 2008.

[4] R. K. Maix et al., “Design, Production and QA Test Results of the NbTi CIC Conductors for the W7-X Magnet System”, *J. Phys.: Conf. Ser.*, vol. 43, pp. 753-758, 2006.

[5] P. D. Weng et al., “Quench current measurement and performance evaluation of the EAST toroidal field coils”, Fus. Eng. Des., vol. 75-79, pp. 143-148, 2005.

[6] L. Zani et al., “Design of JT-60SA magnets and associated experimental validations”, presented at the ASC2010 Conference, to appear in *IEEE Trans. On Appl. Supercond.* 2011.

[7] L. Muzzi et al., “Magnetic and transport characterization of NbTi strands as a basis for the design of fusion magnets”, *IEEE Trans. On Appl. Supercond.*, vol. 19, n0. 3, pp. 2544-2547, 2009.

[8] L. Zani et al., “Jc(B,T) Characterization of NbTi Strands Used in ITER PF-Relevant Insert and Full-Scale Sample”, *IEEE Trans. on Appl. Supercond.*, vol 15, no. 2, pp. 3506-3509, 2005.

[9] A. K. Shikov et al., “The effect of thermo-mechanical treatments on Jc(T,B) and Tcs of Nb-Ti strands”, *IEEE Trans. on Appl. Supercond.*, vol 19, n0. 3, pp. 2540-2543, 2009.

[10] L. Bottura, “Measurement of critical current and magnetization in ITER-relevant Nb-Ti strands”, CERN-ITER Collaboration Report, 2008.

[11] L. Muzzi et al., “Pinning Properties of Nb-Ti Wires Described by a 2-Components Model”, *IEEE Trans. on Appl. Supercond.*, vol 20, no. 3, pp. 1496-1499, 2010.

[12] L. Reccia et al., “Preparation of PF1/6 and PF2 Conductor Performance Qualification Sample”, presented at the ASC2010 Conference, to appear in *IEEE Trans. On Appl. Supercond.* 2011.

[13] P. Bruzzone et al., “Test results of two ITER Poloidal Field Conductor Samples in SULTAN”, presented at the ASC2010 Conference.

[14] L. Affinito et al., “Variable-Temperature characterization of NbTi strands in the low critical-current density range”, *J. Phys.: Conf. Ser.*, vol. 97, p. 012306, 2008.

[15] C. Fiamozzi Zignani, “ENEA Report on SSPF2 testing campaign (April-May 2010)”, June 2010.

[16] R. Zanino et al., “EU contribution to the test and analysis of the ITER poloidal field conductor insert and the central solenoid model coil”, *Supercond. Sci. Technol.* 22, 085006, 2009.

[17] C. P. Bean, “Magnetization of hard superconductors”, Phys. Rev. Lett. 8 p. 250, 1962; C. P. Bean, “Magnetization of high-field superconductors”, *Rev. Mod. Phys.*, vol. 36, p. 31, 1964.

[18] P. Hampshire and D. C. Larbalestier, “The critical current of NbTi multifilamentary wire: A comparison between critical current densities determined using AC magnetization techniques and DC transport measurements throughout the superconducting phase”, *IEEE Trans. Magn.*, vol. 25, p. 1956, 1989.

[19] W. A. Fietz and W. W. Webb, “Hysteresis in Superconducting Alloys – Temperature and Field Dependence of Dislocations Pinning in Niobium Alloys”, *Physical Review*, vol. 178, no. 2, pp. 657-667, 1969.

[20] M. S. Lubell, "Empirical scaling formulas for critical current and critical fields for commercial NbTi", *IEEE Trans. on Magn.*, vol. Mag-19, n0. 3, May 1983.

[21] C. Meingast, and D. C. Larbalestier, “Quantitative description of a very high critical current density Nb-Ti superconductor during its final optimization strain. II. Flux pinning mechanisms”, J. Appl. Phys., vol. 66, n0. 12, pp.5971-5983, 1989.

[22] C. Bormio-Nunes, M. J. R. Sandim, and L. Ghivelder, “Composition gradient as a source of pinning in Nb-Ti and NbTa-Ti superconductors”, J. Phys.: Condens. Matter, vol. 19, pp. 446204-446210, 2007.

[23] A. Augieri et al., “Transport Property Improvement by Means of BZO Inclusions in PLD Grown YBCO Thin Films”, *IEEE Trans. on Appl. Supercond.*, vol 19, no. 3, pp. 3399-3402, 2009.

[24] C. V. Varanasi, P. N. Barnes and J. Burke, “Enhanced flux pinning force and uniquely shaped flux pinning force plots observed in $YBa_2Cu_3O_{7-x}$ films with $BaSnO_3$ nanoparticles”, *Supercond. Sci. Technol.* 20, 1071-1075, 2007.